Characterization, nanoparticle self-organization, and Monte Carlo simulation of magnetoliposomes

Michele Aparecida Salvador
Centro de Ciências Naturais e Humanas, Universidade Federal do ABC, Rua Santa Adelia 166, CEP 09210-170, Santo André, SP, Brazil

Anderson Silva Costa
Instituto de Física, Universidade Federal de Goiás, CEP 74.690-900, Goiânia, Go, Brazil

Marilisa Gaeti, Livia Palmerston Mendes, and Eliana Martins Lima
Faculdade de Farmácia, Universidade Federal de Goiás, CEP 74605-220, Goiânia, Go, Brazil

Andris Figueiroa Bakuzis
Instituto de Física, Universidade Federal de Goiás, CEP 74.690-900, Goiânia, Go, Brazil

Ronei Miotto
Centro de Ciências Naturais e Humanas, Universidade Federal do ABC, Rua Santa Adelia 166, CEP 09210-170, Santo André, SP, Brazil
(Received 31 March 2014; revised manuscript received 14 October 2015; published 29 February 2016)

In this work we have developed and implement a new approach for the study of magnetoliposomes using Monte Carlo simulations. Our model is based on interaction among nanoparticles considering magnetic dipolar, van der Waals, ionic-steric, and Zeeman interaction potentials. The ionic interaction between nanoparticles and the lipid bilayer is represented by an ionic repulsion electrical surface potential that depends on the nanoparticle-lipid bilayer distance and the concentration of ions in the solution. A direct comparison among transmission electron microscopy, vibrating sample magnetometer, dynamic light scattering, nanoparticle tracking analysis, and experimentally derived static magnetic birefringence and simulation data allow us to validate our implementation. Our simulations suggest that confinement plays an important role in aggregate formation.

DOI: 10.1103/PhysRevE.93.022609

I. INTRODUCTION

The synthesis and development of nanoscale structures have attracted a great deal of interest in the biomedical area. This is mainly related to the fact that it is possible to design and produce systems whose size is comparable to important biological structures, such as viruses, proteins, and DNA, and hence can interact directly with them. Magnetic colloids are an interesting example of this class of nanosystem. Magnetic colloids, also known as ferrofluids or magnetic fluids, consist of surface-coated magnetic nanoparticles stably dispersed in a liquid carrier. The choice of the surface coating give rise to both polar or nonpolar magnetic fluids. Those nanofluids have found a broad range of applications including heat and mass transfer applications, such as liquid-cooled loudspeakers and high-power transformers [1–3], magnetophotonics (magnetically controlling backward and forward scattering [4–6]), environmental cleaning through water purification [7], and several biomedical applications. This last topic is probably one of the most appealing research areas and applications on stem-cell labeling [8,9], atherosclerosis detection [10], metastasis diagnostics [11], and even *in vitro* biodetection and *in vivo* cancer treatment [12–16] have already been reported. In fact, the use of magnetic nanoparticles in the biomedical field has increased so much in the last years that this new field is being called biomedical nanomagnetics [17].

The entrapment of these particles by liposome makes them highly dipersible in aqueous media as well as biocompatible. These structures, where a fraction of magnetic nanoparticles are encapsulated into phospholipid vesicles, are known as magnetoliposomes [18]. The importance of magnetoliposomes is mainly related to their use as drug or other therapeutic agent and/or peptide delivery systems and in the diagnosis and/or treatment of diseases [18–22]. The synthesis of magnetoliposomes involves aspects of preparation and stabilization of magnetic fluid and the formation of the multiphasic system, since encapsulation efficiency and the ability of the carrier in maintaining the entrapped substance until the desired target is reached are among the major requirements for therapeutic usage. Therefore, in order to take advantage of the full potential of these systems, it is imperative to control the number of nanoparticles encapsulated [23]. Additionally, all research involving magnetoliposomes so far is restricted to the experimental area. Indeed, the theoretical challenge involved in this study is enormous. First, it is necessary to properly describe the magnetic fluid, a difficult task by itself, as recently described by us [24]. Next, a proper description of the interaction of the liposome bilayer with the nanoparticles must be developed.

Our aim in this work is to devise and implement a numerical method that allows the simulation of magnetoliposomes. To do so, we have developed a new approach where we explicity consider the interactions not only among nanoparticles but also between nanoparticles and the lipid bilayer. In this approach, the interaction among nanoparticles follows the scheme recently described by our group [24], while the interaction between nanoparticles and the lipid bilayer is represented by a ionic repulsion term. This ionic potential is a function of the bilayer-nanoparticle surface electrical potential and depends on the nanoparticle-lipid bilayer distance and the concentration

of ions in the solution. As detailed in the next section, in our model the liposome surface is divided into spheres with size similar to the nanoparticles, and the interaction energy among these *pseudoparticles* and the nanoparticles is represented by an ionic potential. From this model, we investigated the influence of the interaction of the bilayer with the magnetic fluidon characteristics such as the number of particles in an aglomerate and mean aglomerate size. Our numerical data are directly compared to experimental results obtained by our group, using various characterization techniques. Our manuscript is organized as follows: in Sec. II we describe the experimental setup and in Sec. III our Monte Carlo (MC) implementation. Our results are discussed in Sec. IV and our conclusions are presented in Sec. V.

II. EXPERIMENTAL DETAILS

Soybean phosphatidylcholine (PC) Lipoid S100 (1,2-diacyl-sn-glycero-3-phosphocholine), >98% purity, was purchased from Lipoid GmbH (Köln, Germany). Polycarbonate membranes (600-, 200-, and 100-nm pore diameter) were purchased from Whatman (Dassel, Germany). TES buffer was from Sigma (St. Louis, USA). Fe^{+2}, Fe^{+3}, ammonia solution, hydrochloric acid, citric acid sodium salt aqueous solution, potassium hydroxide water solution, and distilled water of analytical grade, used without further purification, were purchased from Merck (Germany), Carlo Herba (Germany), or Synth (Brazil).

For the synthesis of manganese ferrite (MNF) nanoparticles, 50 mmol of $FeCl_3$ and 25 mmol of $MnCl_2$ (both dissolved in 100 mL of HCl 3% w/w) were introduced into 500 mL of boiling 2.0 mol/L methylamine solution under vigorous stirring. After 30 min of reaction, the obtained solid was magnetically separated from the supernatant and washed 3 times with distilled water. The precipitate was acidified with 0.5 mol/L HNO_3 solution and magnetically separated from the supernatant, which was discarded. The nanograins obtained were hydrothermally treated by boiling with 0.5 mol/L $Fe(NO_3)_3$ for 30 min and the excess ferric nitrate was removed from the solution by magnetic decantation. For the elaboration of the magnetic fluid sample, the precipitate was fractioned and nanoparticles peptised in aqueous solution by modifying their surface using sodium citrate, stirring for 30 min, with the mass ratio of 5% between $Na_3C_6H_5O_7$ and $MnFe_2O_4$, in 50 mL of water. The obtained precipitate was magnetically separated and the supernatant disregarded. Afterwards, the precipitate was washed with acetone 3 times, and then the desired amount of water (around 50 mL) was added and the excess of acetone evaporated in order to form the sample. The magnetic colloid was stably dispersed in water under physiological conditions.

Liposomes containing magnetic nanoparticles were prepared by thin lipid film hydration followed by extrusion. In brief, PC was dissolved in chloroform in order to obtain a thin dry film in a round-bottom flask using a rotary evaporator (TE-210, TECNAL, Piracicaba, Brazil). The flask was kept under vacuum for 24 h to ensure complete removal of residual solvent. The dry lipid film was then hydrated with TES buffer (pH 7.0). The dispersion was vortexed and then extruded through 600-, 200-, and 100-nm polycarbonate membranes (Whatman, Dassel, Germany) using a stainless-steel miniextruder (Northen Lipids, Burnaby, Canada) with nitrogen as the pressurizing gas.

Magnetoliposomes formulations were prepared to contain a similar concentration of liposomes, i.e., 50 mM of PC, and distinct amounts of magnetic nanoparticles obtained by changing the amount of magnetic fluid in the preparation. Magnetoliposomes were separated from nonentrapped magnetic nanoparticles in the dispersion by ultrafiltration using a 300 000 MWCO VivaSpin 2 device (Sartorius Stedim Biotech, Goettingen, Germany) with 10 min of centrifugation at 4500*g* at 20 °C.

The liposome size distribution and polydispersity index (PdI) were determined by dynamic light scattering (Zetasizer NanoS, Malvern, Malvern, United Kingdom) with the sample previously diluted in TES buffer.

Nanoparticle tracking analysis (NTA) measurements were used to estimate the liposome concentration and size distribution. NTA was performed with a NanoSight NS500 (Amesbury, United Kingdom), equipped with a sample chamber and a 532-nm laser. Magnetoliposomes were diluted before analysis with TES buffer and automatically loaded into the sample chamber. The software used for capturing and analyzing the data was the NTA 2.3. Video clips of the samples were captured at room temperature by an electron-multiplying charge-coupled-device camera for 215 s, with manual shutter and gain adjustments. The liposome concentration, mean size, and SD values are obtained by analysis of the phoretic mobility of the nanocarriers, i.e., by following the Brownian motion of each individual particle and the use of the Stokes-Einstein relation [25].

Dynamic light scattering (DLS) measurements were performed with a Malvern Zetasizer Nano ZS (Malvern, Herrenberg, Germany) equipped with a 633-nm He-Ne laser and operating at an angle of 173°. The software used to collect and analyze the data was the Dispersion Technology Software version 6.01 from Malvern. Five hundred microliter of each sample were measured in single-use polystyrene half-micro cuvettes (Fisher Emergo, Landsmeer, The Netherlands) with a path length of 10 mm. The measurements were made at a position of 4.65 mm from the cuvette wall with an automatic attenuator and at a controlled temperature of 25 °C. For each sample, 15 runs of 10 s were performed, with three repetitions. The size distribution by intensity and the *Z*-average diameter were obtained from the autocorrelation function using the general purpose mode. The default filter factor of 50% and the default lower threshold of 0.05 and upper threshold of 0.01 were used.

Transmission electron microscopy (TEM) of the manganese ferrite nanoparticles was obtained using a JEOL JEM-2100 (Peabody, MA) microscope operating at 200 kV (resolution 2.5 Å). The experimental size distribution follows a log-normal function and was obtained from the TEM micrographs:

$$g(D) = \left[\frac{1}{\sqrt{2\pi}D\sigma}\exp\left(-\frac{\ln^2\frac{D}{D_o}}{2\sigma^2}\right)\right], \quad (1)$$

where D_o and σ are the median diameter and size dispersion, respectively. Equation (1) was used to fit the TEM size data. The standard deviation was calculated from the fitting

parameters of the lognormal size distribution, i.e., $SD = \sqrt{[\exp(\sigma^2) - 1]D_o^2 \exp(\sigma^2)}$, with a mean diameter value $\hat{D} = D_o * \exp(\sigma^2/2)$.

The manganese-ferrite-based nanoparticles investigated in this work behave as soft magnets, i.e., they have a low magnetic anisotropy, which was found [15] to be $K = 2.5 \times 10^4$ erg/cm^3 from electron magnetic ressonance (EMR) measurements. The Shliomis diameter, i.e., the critical size above (below) which brownian (Neel) relaxation becomes dominant, was estimated to be of the order of 33 nm. From TEM data it is possible to observe that all (or almost all) nanoparticles are below this value. In addition, since the critical value above which the nanoparticles are multi-domain is far larger (around 80 nm, as indicated by Krishnan [17]), it is possible to infer that all the nanoparticles in the assembly are single domain and hence treated under this assumption.

The magnetic characterization was obtained using an ADE vibrating sample magnetometer model EV7. Further, using the VSM data of the colloidal suspensions, we were able to obtain the magnetic particle volume fraction, i.e., the number of nanoparticles per unit volume of the suspension, simply using $\phi = M_s^{\text{fluid}}/M_s^{\text{particle}}$.

For noninteracting monodisperse nanoparticles the magnetization of the colloid follows the well-known Langevin behavior, i.e., $M = \phi M_s L(\xi)$, where $\phi = \frac{N\pi D^3}{6}$, with N the number of magnetic nanoparticles per unit volume; $L(\xi) = \coth(\xi) - \frac{1}{\xi}$ is the Langevin function with $\xi = \frac{\mu_0 \pi M_s D^3 H}{6kT}$, where μ_0 is the vacuum permeability; M_s is the particle saturation magnetization; H is the applied magnetic field; k_B is the Boltzmann constant; and T is the absolute temperature. In the low-field limit, the initial susceptibility is given by $\chi_L = \frac{\pi \phi M_s^2 D^3}{18 k_B T}$ (this term is usually referred to as the Langevin susceptibility). For a polydisperse system the magnetization (M_L) is given by

$$M_L = \frac{\pi N M_s}{6} \int L(\xi) D^3 g(D) dD.$$

Several models were developed to include the effect of particle-particle interaction in the magnetization curve [26]. In particular, the second-order modified mean-field model developed by Ivanov and Kuznetsova [26], successfully applied to magnetic fluids, was chosen by us as a first approximation. In this model, an effective field rather than the applied field is considered:

$$H_e = H + \frac{1}{3} M_L(H) \left\{ 1 + \frac{1}{48} \frac{dM_L(H)}{dH} \right\}.$$

The initial susceptibility is now accordingly rewritten as

$$\chi = \chi_L \left\{ 1 + \frac{1}{c} \chi_L + \frac{1}{144} \chi_L^2 \right\}.$$

Although magnetization studies, and in particular initial susceptibility ones, had been widely used to investigate the effect of particle-particle interaction [24], an effect on the initial susceptibility is only observed at quite high particle volume fractions (greater than 7–9%) [26,27]. As discussed later, these observations do not imply that aggregate formation starts only at high concentration.

The amount of magnetic nanoparticles per liposome is obtained by dividing the number of magnetic nanoparticles per milliliter (from VSM analysis) by the number of liposomes per milliliter (obtained from NTA analysis). In this approximation, we assumed that there is no leaking of nanoparticles from the liposomes within the experimental window time, i.e., considering the whole window time between the magnetoliposome preparation and the acquisition of the magneto-optical experimental data, which is typically shorter than 48 h. Previous stability analysis of magnetoliposome dispersions indicated that size distribution of the nanocarriers did not change within 7 days for samples maintained at both 25 °C and 4 °C. However, it is important to mention that this is not a general feature. Indeed, we have already [23] observed up to 50% of leakage after 48 h of the loading of the carboxyldextran-coated magnetite nanoparticles inside the liposomes. The main difference between this previous observation and the new experimental procedure is that the former nanoparticles were prepared through the sonication method.

The room-temperature static magnetic birefringence (SMB) data were obtained using the traditional lock-in detection technique [4,23]. The experimental setup consists of a chopped laser beam (632 nm) of 10 mW crossing the sample cell perpendicularly before illuminating the photodetector. The sensitivity of the photodetector was 3.5 mV μW^1 cm^2. The flat quartz sample cell has a sample thickness (L) of 2.0 mm. Both the polarizer and analyzer are attached to a goniometer device that allows full angular rotation. The sample cell is mounted in the gap of an electromagnet so the laser beam and the external magnetic field are mutually perpendicular. The axes of the polarizer and analyzer are set perpendicular to each other, forming an angle of $\frac{\pi}{4}$ in relation to the magnetic field direction during SMB measurements. Also, an absorption filter is positioned before the polarizer with the purpose of decreasing the light transmission and avoiding thermodiffusion effects [28]. In the absence of dichroic contributions, the light intensity obtained in the detector is given by

$$I = I_0 \sin^2 \frac{\pi L \Delta n}{\lambda}$$

with I_0, L, and λ related to the incident light intensity, the sample thickness, and the laser wavelength, respectively. Δn is the magnetic birefringence given by the following equation [23,29]:

$$\Delta n = \frac{\pi n_0 N_Q Q}{12} (\chi_{zz} - \chi_{xx})_Q \int D^3 L_2(\xi_Q) g(D) dD, \quad (2)$$

where N_Q is the number of nanoparticle chains per unit of volume, n_0 is the refraction index of the liquid carrier, and $\chi_{zz}(\chi_{xx})$ is the effective electrical susceptibility of the magnetic nanoparticle chain parallel (perpendicular) to the anisotropy axis [30]:

$$\chi_{zz} = \frac{1}{Q} \sum_{i=1}^{Q} \frac{\chi_o}{1 - \kappa_{zzi} \chi_o}$$

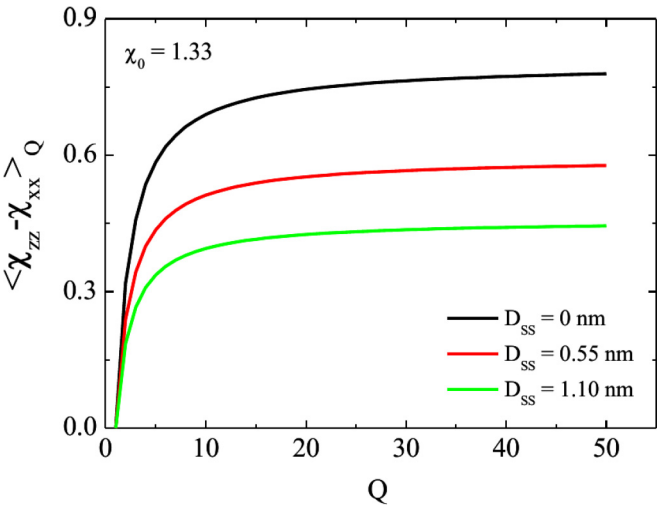

FIG. 1. Difference between the effective electrical susceptibility of the magnetic nanoparticle chain in the parallel and perpendicular directions ($\chi_{zz} - \chi_{xx}$) as a function of the chain size (Q) for different surface-to-surface particle distance (D_{ss}) values.

and

$$\chi_{xx} = \frac{1}{Q}\sum_{i=1}^{Q}\frac{\chi_o}{1+\kappa_{xxi}\chi_o}$$

with

$$\kappa_{xxi} = 2\kappa_{zzi}$$

and

$$\kappa_{zzi} = \frac{1}{3}\left(\frac{D}{D+D_{ss}}\right)^3\sum_{j\neq i}\frac{1}{|j-i|^3}.$$

The electrical susceptibility of the nanoparticle is assumed to be the same value as for magnetite [4] $\chi_o = 1.33$.

From Fig. 1, it is clear that the difference $\chi_{zz} - \chi_{xx}$ is strongly influenced by both surface-to-surface particle distance (D_{ss}) and agglomerate chain size (Q). It is also interesting to point out that the saturation value increases for lower D_{ss}.

In Eq. (2),

$$L_2(\xi_Q) = 1 - \frac{3}{\xi_Q}L_1(\xi_Q)$$

is the second Langevin function, with $L_1(\xi_Q) = \coth\xi_Q - \frac{1}{\xi_Q}$ and $\xi_Q = \frac{\mu_0 Q\pi M_s D^3 H}{6kT}$, already defined earlier.

SMB data were adjusted following

$$I = I_0^{\exp}\left[\sin^2\left(\Delta n_s\int L_2(\xi_Q)D^3 g(D)d(D)\right)\right], \quad (3)$$

where only Δn_s and Q are adjustable parameters, since $g(D)$ is obtained from the polydispersity of the dried nanoparticles. While Q represents the mean agglomerate size, the adjusted magnetic birefringence, Δn_s, is related to the effective electrical susceptibility of the magnetic nanoparticle chain

$$\Delta n_s = \frac{\pi^2 n_0 L Q N_Q}{12\lambda}\langle\chi_{zz} - \chi_{xx}\rangle_Q.$$

Note that this technique allows us to extract the number of particles ($Q * N_Q$) contributing to the static magnetic birefringence signal. If the nanoparticles are perfect spheres, then only agglomerated particles will contribute to the SMB signal.

Our magnetic birefringence model is similar to the one proposed by Xu and Ridler [30]. The main difference is in the fact that we assume a mean agglomerate size instead of considering separately each aggregate structure and summing all contributions with their particular fraction amount. This procedure decreases the number of fitting parameters and might better represent average characteristics of the sample. It is also important to mention that the SMB model considered is valid at low particle concentration, which is the experimental situation in this work. For high particle concentrations a more general model, such as the one proposed by Rasa [27], must be considered.

It is important to point out that among the the techniques considered in this work, the magneto-optical setup is the most powerful experimental technique to investigate aggregate formation. This is because in birefringence experiments only a fraction of nanoparticles (mainly the ones that form aggregates) contribute to the signal. In contrast, in other techniques, such as initial magnetic susceptibility studies in magnetization curves, all the nanoparticles contribute to the detecting signal (magnetic moment). Therefore, since in our samples the nanoparticles encapsulated into liposomes are not at high particle concentration, the static magnetic birefringence (and not necessarily the magnetization analysis) is expected to play a significant role in the validation of our Monte Carlo simulations.

III. MONTE CARLO SIMULATIONS OF MAGNETIC FLUIDS

The stability of a magnetic fluid is a balance between attractive forces, such as magnetic dipolar and van der Waals, and repulsive ones, like steric and ionic repulsion. When the target system is a magnetoliposome, it is also important to consider the interaction between the nanoparticles and the lipid bilayer. Since this is our target sample, our systematic comparison between experimental and theoretical data will allow a better understanding of the role of the lipid bilayer in key structural parameters, such as agglomerate size, mean particle-particle distance, and magnetization. The size of magnetoliposomes restricts quantum chemistry calculations involving these systems, and therefore we have chosen Monte Carlo simulations as our simulation tool.

Monte Carlo [31] is a label used to designate stochastic methods for solving mathematical problems. Systems that follow the Boltzmann energy distribution can be simulated by means of the Metropolis algorithm [32,33], which starts from a random configuration of the system and performs successive small variations in all its coordinates. The procedure is as follows: (a) For each variation, the change $\triangle E$ in energy is calculated; (b) if the value of the new potential energy is lower than the previous one, then the new configuration is accepted; and (c) if the new potential energy is higher, then a random number between 0 and 1 is generated and then compared

with the factor $e^{\frac{-\Delta E}{k_B T}}$, where k_B is the Boltzmann constant. In this latter case, the new configuration is accepted only if the random number is lower than this factor. The steps [from (a) to (c)] are then repeated, and, after a period of stabilization of the energy, the average values of the properties of interest are computed considering all accepted configurations. This procedure guarantees that the accepted configurations follow the Boltzmann energy distribution, $ke^{\frac{-E}{k_B T}}$, where k is an arbitrary constant and E is the systems energy. Following the Markov chain method of sampling [34], the calculated average values represent the expected values of the respective properties under investigation.

Since magnetic fluids are characterized by a large number of coupled degrees of freedom, MC simulations have early been chosen as a possible way of exploring its properties. For a critical review on the evolution of MC use in the description of magnetic fluids see Ref. [24]. The basic principles of our Monte Carlo simulations were already discussed in detail [24,35]. In these works, our MC implementation for an ionic-surfacted magnetic fluid model is extensively compared not only to dipolar soft matter studies but also to simulations where other kinds of interactions are included. Therefore, our discussion in this matter will be brief: We first point out the main features of our calculations and later introduce the changes we have made in order to properly treat magnetoliposomes.

In the following discussion, a Monte Carlo step (MC step) indicates that a given configuration of nanoparticle's has its position and magnetic moments randomly changed in order to generate a new configuration. In this study our target structures are composed by magnetoliposomes, i.e., nanoparticles trapped in a 150-nm diameter lipid bilayer. The magnetic nanoparticle diameters follow a log-normal distribution, Eq. (1). By means of a stochastic method [36], our program generates a sample of N diameters that follows this distribution where each single diameter differs. The number of nanoparticles is directly related to the magnetic nanoparticle's volume fraction. Since the process to achieve a given volume fraction is based on random numbers, the total number of nanoparticles for different ensembles of a given concentration might slightly differ.

The net interaction potential (U_{total}) between a pair of ionic-surfacted magnetic nanoparticles (i and j, as represented in Fig. 2) is obtained by summing the individual terms over all considered pairs:

$$U_{\text{total}}(ij) = U_m(ij) + U_w(ij) + U_s(ij) + U_i(ij) + U_B(ij), \tag{4}$$

where U_m is the magnetic dipolar interaction, U_w the van der Waals interaction, U_s the steric repulsion, U_i the ionic repulsion, and U_B the Zeeman interaction.

The *magnetic dipolar interaction* is given by:

$$U_m(ij) = \frac{\mu}{4\pi}\left[\frac{\vec{m}_i \cdot \vec{m}_j}{r^3} - 3\frac{(\vec{m}_i \cdot \vec{r}_{ij})(\vec{m}_j \cdot \vec{r}_{ij})}{r^5}\right],$$

where μ is the magnetic permeability of the solvent, in our case very close to the vacuum value; $\vec{m}_i$ and $\vec{m}_j$ are the magnetic dipole moment vectors of the particles i and j, respectively;

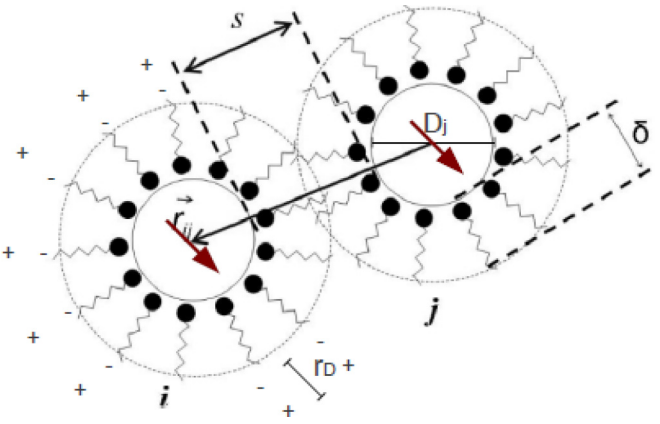

FIG. 2. Illustration of two ionic-surfacted magnetic nanoparticles, with surfactant molecules adsorbed on their surfaces. For simplicity, the ionic double layer is not shown. Each surfactant molecule is composed of an apolar chain that work as a *bridge* between the adsorbed and the ionized polar heads. D_i and D_j are the diameters, $\vec{m}_i$ and $\vec{m}_i$ are the magnetic dipole moment vectors, δ is the effective length of the surfactant molecules, $\vec{r}_{ij}$ is the relative position of the center of the nanoparticle i in relation to that of nanoparticle j, s is the perpendicular distance between the surfaces of the nanoparticles, and s' is the perpendicular distance between the surfaces formed by the ionized polar heads of the nanoparticles. R_D, the *Debye radius*, is the estimation of the length of the ionic layer.

the vector $\vec{r}_{ij}$ is position of i in relation to j; and r is the modulus of $\vec{r}_{ij}$. The magnitude of $\vec{m}$ is calculated by the product $M_s V$, where M_s is the intrinsic spontaneous magnetization and V the volume of the nanoparticle. As M_s and V are constant for a given nanoparticle, changes in the magnetic dipole moments in different MC steps are simply given by three-dimensional rotations. It is very important to mention that, although this term can be depicted as magnetically hard point dipoles with translational and rotational degrees of freedom, we have clearly shown [24] that dipolar interactions are dominant only for large nanoparticles or for systems where the nanoparticles are far apart. Therefore, other types of interactions are considered, as discussed below, specially due to their relevance in aggregate formation in particular for low particle sizes [24].

The *van der Waals interaction* is described by the potential [37]

$$U_w(ij) = -\frac{A}{12}\left[\frac{D_{ij}^2}{r^2} + \frac{D_{ij}^2}{r^2 - D_{ij}^2} + 2ln\left(\frac{r^2 - D_{ij}^2}{r^2}\right)\right],$$

where A is the Hamaker constant, and D_{ij} is the mean of the diameters of the nanoparticles i and j [$D_{ij} = (D_i + D_j)/2$]. As we have discussed before [35], and according to the *Lifshitz theory* [38–40], the Hamaker constant for this system can be describe in terms of macroscopic characteristics of the nanoparticles and the solvent as

$$A \approx \frac{3}{4}k_B T\left(\frac{\varepsilon_{Fe_3O_4} - \varepsilon_{H_2O}}{\varepsilon_{Fe_3O_4} + \varepsilon_{H_2O}}\right)^2 + \frac{3h\nu_e}{16\sqrt{2}}\frac{\left(\eta_{Fe_3O_4}^2 - \eta_{H_2O}^2\right)^2}{\left(\eta_{Fe_3O_4}^2 + \eta_{H_2O}^2\right)^{3/2}}, \tag{5}$$

where h is the Planck constant, $\varepsilon_{Fe_3O_4}$ is the electric permittivity of magnetite (nanoparticles), ε_{H_2O} is the electric permittivity of water (solvent), $\eta_{Fe_3O_4}$ and η_{H_2O} are the corresponding indexes of refraction, and ν_e is the main absorption frequency, considered the same for both magnetite and water in this approximation. For a temperature $T = 30\,^{\circ}\mathrm{C}$, we have that $\varepsilon_{H_2O} = 76.6$ [41,42] and $\eta_{H_2O} = 1.40$ [41,43]. The value of ν_e for magnetite has been estimated to be between 0.3 and 3.0×10^{15} Hz [44]. Using Eq. (5), this leads to Hamaker constants between 10^{-19} and 10^{-20} J.

The *steric repulsion*, in its turn, is described by the potential [45]

$$U_s(ij)=\begin{cases}\frac{\pi\xi k_B T}{2}D_{ij}^2\left[2-\frac{l}{t}-\frac{l+2}{t}\ln\left(\frac{1+t}{1+\frac{l}{2}}\right)\right] & \text{if} \quad (s/2\delta)\leqslant 1\\ 0 & \text{if} \quad (s/2\delta) > 1\end{cases},$$

where ξ is the *grafting* (surface density of adsorbed molecules in the nanoparticles), deeply studied in previous works [35,46], s is the perpendicular distance between the nanoparticles' surfaces, and δ is the surfactant layer width, $l = 2s/D_{ij}$ e $t = 2\delta/D_{ij}$. When each one of these molecules presents free charge at its extremities, there is also an ionic repulsion.

The *ionic repulsion* is described by the potential [38]

$$U_i(ij) = 64\pi k_B T \rho_\infty \gamma_i \gamma_j \frac{D_i D_j}{D_i + D_j} R_D^2 e^{-s'/R_D}, \qquad (6)$$

where ρ_∞ is the ion concentration in a point infinitely far from the surfaces; D_i and D_j are the diameters; s is the distance between the surfaces; γ_i and γ_j are given by

$$\gamma_i = \tanh\frac{e\psi_s(i)}{4k_B T}, \quad \text{and} \quad \gamma_j = \tanh\frac{e\psi_s(j)}{4k_B T}, \qquad (7)$$

where $\psi_s(i)$ and $\psi_s(j)$ are the electrical potentials at the surfaces of the nanoparticles i and j; and R_D is the so-called *Debye radius*, given by

$$R_D = \left(\frac{\varepsilon k_B T}{\rho_\infty Z^2 e^2}\right)^{\frac{1}{2}}, \qquad (8)$$

where ε is the electric permittivity of the solvent and Z is the valency of the ions in the solvent. Finally, each nanoparticle may also interacts with an applied magnetic field by the well-known *Zeeman interaction*, described by the potential

$$U_B(i) = -\vec{m}_i \cdot \vec{B}. \qquad (9)$$

Although our methodology is able to address different values of magnetic field, in the present work only $B = 0$ and $B = 0.3$ T simulations are considered.

It is worth pointing out that, although we have included all the relevant energy terms usually taken in consideration in ferrofluids simulations, we have neglected the magnetic anisotropy energy contribution. Its inclusion would probably allow us to extract magnetization curves that are closer to the experimental ones. However, in this work we will not address this issue, although we plan to do so in the near future. So far, our simulation focus has been mainly in the study of aggregate formation [24,35]. For this purpose we are convinced (at least for low particle sizes) that our simulation does represent very well this system. We have found and extensively discussed (see, for example, Ref. [24]) that, at this size range (i.e., low dipolar interaction), the van der Waals and the ionic-steric terms are dominant when aggregate formation is the main concern. So, independent of considering explicitly the magnetization rotation without particle rotation, the aggregate configuration is expected to be the same for parameters in the range considered in our investigations.

As described in detail in previous works [24,35], our Monte Carlo implementation starts from a random configuration of the considered nanoparticles [subject to the interactions in Eq. (4)] and performs successive small variations in all its coordinates. For the magnetic fluid system simulated in this work, a configuration is determined by the positions of the nanoparticles and the orientations of its magnetic dipole moments. Therefore, in each iteration of the Metropolis algorithm, both the positions and the orientations of the magnetic dipole moments of all considered nanoparticles experience a random change. In each simulation the number of nanoparticles were adjusted to precisely achieve the desired particle volume fraction considering a liposome with a fixed radius of 150 nm.

In our analysis two nanoparticles are considered as being part of the same agglomerate if their surface-to-surface distance is less than the sum of their surfactant molecule lengths and their Debye radius values. For two nanoparticles with the same surfactant molecule length and the same Debye radius value, this condition is written as $s \leqslant 2\delta + R_D$. This agglomerate-belonging condition based on proximity was detailed discussed [24] and found to be a good approximation in our simulation-experience comparison.

The ionic-surfacted layer is composed of two parts: the surfacted layer, which provides steric repulsion when two of them are in contact, and the ionic layer, which is itself a double layer of ions and counterions that provides an ionic repulsion between the nanoparticle pair. It is clear that both interactions are correlated, as their microscopic origin is the same: the adsorbed layer. In order to build up a model that relates these repulsions, we assume [24] that each surfactant is adsorbed radially in the nanoparticle and its polar head stays at a certain distance from the nanoparticle surface. In such case, a effective charge density, with spherical format, provides ions with a charge opposed to the charge of the electrolyte solution.

Considering that each ionized extremity presents a charge $z_s e$, the relation between the charge density (ς) can be written as a function of the grafting (ξ) [24]:

$$\varsigma = \left[z_s e \frac{R^2}{(R+\delta)^2}\right]\xi, \qquad (10)$$

where R is the radius of the nanoparticle and δ is the width of the ionic-surfacted layer.

Following these assumptions, we can model the ionic-surfacted layer as the superposition of the steric and ionic repulsion potentials and use relation 10 to write the ionic repulsion's parameters that depends on ς as functions of ξ. As in our model each nanoparticle i has a different radius, it is clear that their surface charge densities (ς_i) also differ and hence any properties related to ς_i should be individually

TABLE I. Surface electric potential ψ_s (equivalent to the so-called ζ *potential*) and the charge density ς for selected values of *grafting* ξ for the target system considering $\overline{D} = 13.32$ nm and $\delta = 0.55$ nm.

$\xi(m^{-2})$	ψ (V)	$\zeta(\mathrm{C/m^2})$
0.06×10^{18}	-1.55×10^{-2}	-0.81×10^{-2}
0.12×10^{18}	-2.99×10^{-2}	-1.62×10^{-2}
0.18×10^{18}	-4.20×10^{-2}	-2.44×10^{-2}

computed. This is done considering the relations

$$\{\psi_s\}_i = -\frac{k_B T}{e}\mathrm{acosh}\left(1 + \frac{\{\varsigma\}_i^2}{4\varepsilon k_B T \rho_\infty}\right), \tag{11}$$

$$\{R_D\}_i = \left\| \frac{\varepsilon\psi_0}{\{\varsigma\}_i} \right\|, \tag{12}$$

and

$$\{\gamma\}_i = \tanh\left(\frac{Ze\{\psi_0\}_i}{4k_B T}\right), \tag{13}$$

as functions of ξ using Eq. (10).

Both the nanoparticle surface electric potential ψ_s (equivalent to the so-called ζ potential) and the charge density ς are linked to the *grafting* ξ, to the diameter D, and to the surfactant molecule effective length δ. Table I shows ψ_s and ς as a function of ξ for selected graftings considering $\overline{D} = 13.32$ nm and $\delta = 0.55$ nm. It is interesting to note that our estimated values for both ψ_s and ς are inside or near experimentally observed ranges [47–49]: ψ_s between 20 mV and 85 mV and ς around 0.1 $\mathrm{Cm^{-2}}$, frequently reaching 0.3 $\mathrm{Cm^{-2}}$.

The experimental value of the ζ potential was obtained from electrophoretic mobility measurements performed by phase analysis light scattering using ZetaSizer Nano ZS equipment (Malvern Instruments, Malvern, UK). Measurements were performed after sample preparation revealing a ζ potential of -28 mV. According to our theoretical analysis, this corresponds to a grafting around 0.22 $\mathrm{nm^{-2}}$.

Finally, it is important to stress that our model was extensively tested not only by us [24,35] but also by other groups [50] for different types of nanoparticles in different conditions.

A. The nanoparticle: Lipid bilayer interaction model

Usually the interactions between the lipid bilayer surface and the surrounding liquid are described by van der Waals, Coulomb, hydration, and steric potentials. In colloidal systems, on the other hand, rarely more than two of those interaction potentials are considered [38]. In the formation of miceles, bilayer, and liposomes, the auto-organization of amphiphilic molecules is mainly governed by hydration and hydrophobic interactions [51]. In complex systems, such as the magnetoliposomes considered in the present work, all these interaction potentials might play a crucial role in the system's properties. Indeed, a number of other specific interactions, such as adhesion, ligant-receptor, and other interface reactions might be present [38]. In the following we briefly analyze the contribution of some of these interaction potentials in our target system.

The van der Waals interactions among amphiphilic molecules and their derived structures are relatively weak. This is because the Hamaker constant [A, in Equation (5)] between hydrocarbon radicals and water is at least one order of magnitude smaller than the typical values observed for magnetic colloids: $4 - 7 \times 10^{-21}$ J for the former against $6 - 20 \times 10^{-20}$ J for the latter [38].

The hydration interaction between phospholipid bilayers was recently found [52] to be of very short range. The molecular dynamic simulations of Kanduc, Schneck, and Netz [52] indicated that hydration interaction in phospholipd bilayers present an exponential decay, with a decay length of the order of 0.4 nm. This is consistent with the fact that, in the scale of the water molecule, the phospholipid bilayer does not present a smooth interface and hence water molecules are not expected to be in an ordered phase.

The electrostatic repulsion, on the other hand, presents a more long-range character. Although electrostatic interactions in complex systems like magnetoliposomes might be very sensitive to the pH, surface potential and the type and concentration of the electrolytes in the solution, their long-range character suggest that they have a key role in the properties of these systems. Following this assumption, in our model the interaction between the liposome surface and the magnetic nanoparticle is basically governed by electrostatic repulsion as described by the Gouy-Chapman [38,53,54] approximation. This choice is based on the experimental observation by Aguilella *et al.* [55]. In their work, Aguilella *et al.* found that differences between the experimental measured surface charge density of charge lipid layers and the Gouy-Chapman approximation could be explained if the area per lipid molecule, the pH, and the dependence between the dissociation degree and concentration were taken in consideration. Aguilella *et al.* [55] have found that the surface potential ψ_0 between the interface and the electrolytic solution is given by

$$\psi_0 = \frac{2RT}{F}\arcsin(f\alpha), \tag{14}$$

where

$$f = -e[A^2 4RT\varepsilon\varepsilon_0\rho)]^{-1/2}, \tag{15}$$

and R and F are the ideal gas and the Faraday constants, respectively, A is the lipid polar head group area, ε is the dielectric constant, ε_0 the vacuum permittivity, ρ the concentration of ions, and α the degree of lipid dissociation. This results were found to be consistent with the experimental data obtained by Taylor and coworkers [56] for surface potential measurements on stearic acid monolayers.

In order to proper apply this approximation to our target system, in our model, the phospholipid bilayer is represented by pseudoatoms, as is usually done in coarse-grained calculations [57]. Coarse-grained calculations are basically reduced models which retain close connections to the underlying atomistic representation. A common pattern employed by many simulation methods is lumping groups of atoms together into a single interaction site [57] or pseudoatoms. The coarse-grained approach is widely used in studies of lipid bilayers, where the lipids are divided in a few interaction sites. The number of interaction sites, the system's size and the interaction potentials used might have several consequences

in the model's capability of properly describing the system's properties [58]. In our approach, the phospholipid bilayer is represented by a single interaction site or pseudoatom. This choice is mainly justified by the size of our system and the interaction potential considered. Each pseudo-atom interacts with the magnetic nanoparticles by an ionic potential described by Eqs. (14) and (15) connected with Eqs. (6) and (7). It is also important to mention that this model needs further improvements in order to address PEGylated liposomes, such as those studied by Amstad and coworkers [59].

B. Simulated system

In the next section, all simulations are performed considering the following parameters: ion concentration in the solution, $\rho = 0.05$ mol/L; electric permittivity $\varepsilon = 7.09 \times 10^{-10}$ C^2/Nm^2, magnetic permeability $\mu = 1.26$ N/A^2; particle volume fraction, $\phi = 0.0075 \rightarrow 0.050$; median diameter, $D_0 = 12.7$ nm; diameter dispersion, $\sigma = 0.31$; surfactant layer thickness, $\delta = 0.55$ nm; Hamaker constant, $A = (5 - 20) \times 10^{-20}$ J; and grafting, $\xi = 0.22 \times 10^{18}$ m^{-2}. A giving Monte Carlo step is characterized by the positions and magnetic moments of the nanoparticles distributed inside the liposome. Although our experimental data (see next section) indicates that the liposome diameters are around 150 nm, in all simulations the liposome diameter considered is around 100 nm. This choice is made in order to guarantee that the number of nanoparticles is not very small, especially for small particle volume fraction concentrations and, at the same time, the size of our simulated magnetoliposome is no smaller than the experimental samples considered. In other words, the liposome size is chosen in order to guarantee that the minimum number of trapped nanoparticles is statistically significant and at the same time only a small amount of experimental data is collected below this limit.

In order to carry out simulations involving a fixed number of particles, the distribution must be discretized. We have tested our discretization scheme following the proposal of Ivanov [26]. In this approach the moments $\frac{\langle D^n \rangle}{D_0^n}$ of the discretized simulation distribution $g_{\text{discrete}}(D)$ considering 1000 particles and the exact distribution $g(D)$ [Eq. (1)] are compared. The moments obtained from our discrete simulation and the exact distribution are presented in Table II. The deviations do not follow a definite pattern and are always lower than 15%. Since the magnetization is proportional to the third-order moment while the susceptibility is proportional to the sixth order, we expect quantitative deviations between the experimental and simulated values, as discussed latter. This is because in order to simulate the considered size magnetoliposomes and the nanoparticle's concentration range the number of nanoparticles entrapped is usually around 100 or less. In this limit, deviations of the sixth-order moment were found to be higher. Since Kumar *et al.* [50] have extended our previous calculations [35] for FM considering 200 nanoparticles up to 2000 nanoparticles and found only small numerical differences, we understand that our choices for the MC simulations will correctly represent the target system.

TABLE II. The first six moments $\frac{\langle D^n \rangle}{D_0^n}$ of the discretized simulation distribution and the exact distribution defined in Eq. (1). Deviations between the simulation and exact values in percentage are also shown.

Order	1	2	3	4	5	6
Exact	1049	1212	1541	2157	3323	5683
Discrete	1106	1321	1690	2294	3274	4876
Deviation (%)	5.4	9.0	9.7	6.3	−1.5	−14.3

IV. RESULTS

Figure 3 (right) shows the TEM image of the manganese ferrite citrate-coated nanoparticles. In this image it is possible to observe the size dispersity and spherical-like shape of the synthesized nanoparticles. In the inset in Fig. 3 (right), the derived experimental histogram data obtained from several

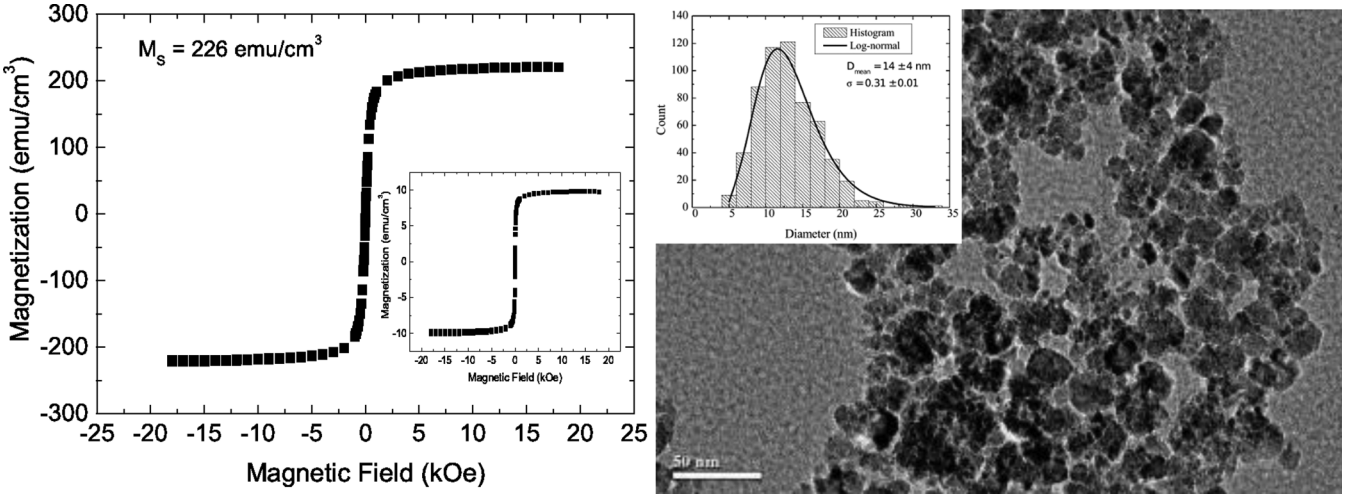

FIG. 3. Right: Transmission electron microscopy (TEM) image of the manganese ferrite citrate coated nanoparticle. Inset: Histogram data derived from TEM image and lognormal fit of the distribution. Left: Specific magnetization curve of the dried (powder) nanoparticles. Inset: Magnetization curve of the magnetic nanoparticle sample. The specific saturation magnetization of the nanoparticle was found to be 44.3 emu/g, which corresponds to a saturation magnetization of 226 emu/cm^3 (226 kA/m).

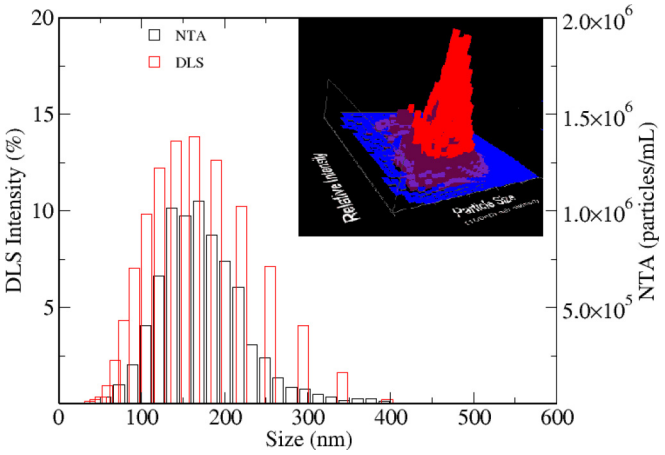

FIG. 4. Size distribution from nanoparticle tracking analysis (NTA) and dynamic light scattering (DLS) measurements of the liposome sample with the corresponding 3D graph (size vs intensity vs concentration; inset).

images, as well as the theoretical fit of log-normal size distribution. Our data indicates that our sample is composed of nanoparticles with a mean diameter $\hat{D} = 14$ nm with a standard deviation SD $= 4$ nm. In Fig. 3 (left) the magnetization curve of the dried (powder) ferrite nanoparticles at room temperature is shown. The specific saturation magnetization of the nanoparticle was found to be 44.3 emu/g, which corresponds to a saturation magnetization of 226 emu/cm^3 (226 kA/m). This soft-ferrite does not show any coercivity at this experimental condition, indicating a superparamagnetic-like behavior. The inset in Fig. 3 (left) shows a typical magnetization curve of a magnetic colloid sample. From the saturation magnetization value of the colloid it is possible to extract the particle volume fraction of the colloid (0.9%). It is important to mention that these magnetic properties were obtained before the magnetic nanoparticles were trapped in the liposome.

In the next step of our investigation, NTA and DLS measurements were used to estimate the liposome concentration and size distribution. Figure 4 presents a comparison between NTA and DLS data obtained for a liposome sample. In the inset a representative 3D graph indicating size as a function of intensity and concentration is also shown. Both techniques showed good sizing accuracy and relatively narrow distributions in agreement with previous systematic investigations [25].

In Table III NTA- and DLS-derived diameter size (d), standard deviation (SD), concentration in liposomes per mL, Z-average diameter, and polydispersity index (PdI) are presented. The samples are named, 200 and 100 nm, after the diameter of the polycarbonate membranes pores they were extruded and X μL according to the amount of magnetic fluid added to the formulation. In the majority of samples considered, the liposome diameters are around 150 nm. As expected, for almost all samples, the mean size values obtained by NTA are slightly smaller than the Z average given by DLS.

Figure 5 shows the static magnetic birefringence of the magnetoliposomes as a function of the magnetic field for different encapsulated magnetic nanoparticle concentrations considering (a) 100 nm and (b) 200 nm liposome samples. The symbols represent the experimental data while the solid lines are the best fit using Eq. (3) with only two fitting parameters: Δn_s and Q.

Using the SMB data we extract the mean chain size Q and the fraction of agglomerates for the liposome formulation. Experimentally, the fraction of monomers and aggregates (dimers, trimers, and high other agglomerates) is obtained from the ratio of nanoparticles contributing to the SMB signal and the total number of particles obtained from the magnetization data for the liposome. Figure 6 shows the SMB data (circles) for the 200-nm sample and the Monte Carlo simulation results (squares). As previously found by our group [46] the higher the particle concentration the lower is the fraction of isolated nanoparticles (monomers). It is also clear that the simulated data is in good agreement with the experimental results, indicating that our MC implementation properly describe this property.

In the inset of Fig. 7, the inverse of the agglomerate mean value $(1/Q)$ as a function of the particle volume fraction is shown for magnetoliposome experimental data black spheres (200 nm) and blue squares (100 nm) and Monte Carlo

TABLE III. Diameter size (d), standard deviation (SD), concentration in liposomes (lip.) per mL, Z-average diameter, and polydispersity index (PdI) obtained using nanoparticle tracking analysis (NTA) and dynamic light scattering (DLS) techniques for different liposome formulations.

	Technique				
Formulation	NTA d (nm)	NTA SD (nm)	NTA lip./mL	DLS Z average (nm)	DLS PdI
Lip. 200 nm + 10 μL PM	168.6	47.6	4.2246×10^{13}	148.1	0.048
Lip. 200 nm + 25 μL PM	160.2	45.8	3.212×10^{13}	150.4	0.058
Lip. 200 nm + 50 μL PM	167.0	47.4	3.3848×10^{13}	143.2	0.061
Lip. 200 nm + 75 μL PM	161.4	45.8	3.3136×10^{13}	138.9	0.091
Lip. 200 nm + 100 μL PM	172.2	50.6	3.7899×10^{13}	139.4	0.125
Lip. 100 nm + 10 μL PM	140.0	48.2	3.7456×10^{13}	110.0	0.048
Lip. 100 nm + 25 μL PM	131.8	40.4	4.7696×10^{13}	106.7	0.062
Lip. 100 nm + 50 μL PM	203.0	59.4	5.6328×10^{13}	105.1	0.078
Lip. 100 nm + 75 μL PM	137.0	48.0	4.6344×10^{13}	102.7	0.064
Lip. 100 nm + 100 μL PM	144.6	51.0	4.9848×10^{13}	105.4	0.097

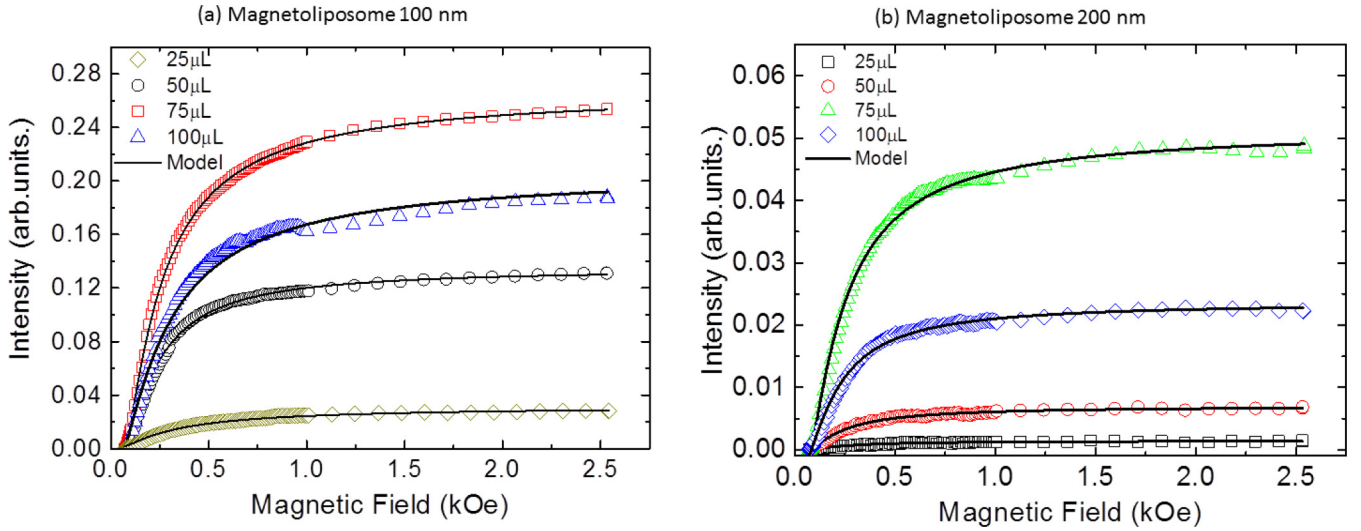

FIG. 5. Static magnetic birefringence of the magnetoliposomes as a function of the magnetic field for different encapsulated magnetic nanoparticle concentrations.

simulations (red hexagons). The experimental data are derived from SMB analysis as discussed in Sec. II. As expected, we observe the increasing of the agglomerate size Q when the number of encapsulated nanoparticles inside the liposome increases. Although some variations can be noted, again the Monte Carlo simulations show the same behavior observed for the experimental data. In order to allow a better visualization, in the next analysis only 200-nm ML-derived data will be shown.

Our experimental analysis is devoted to the investigation of low particle volume fraction samples. In this regime we expect that a chain model might give an insight about aggregate formation. At high concentrations, on the other hand, this approach is probably less accurate, especially due to the formation of more complex self-organized structures. One of the first models designed to access the chain size concentration

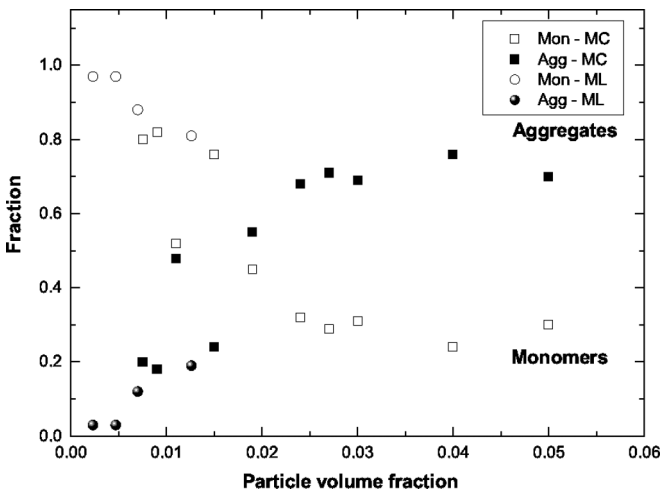

FIG. 6. SMB derived fraction of agglomerates (closed circles) and monomers (closed squares) for the 200-nm sample and Monte Carlo simulation results (open circles and squares). Aggregates indicates dimers, trimers, and high-order clusters.

dependence was the rigid chain model developed by Tsebers [61] and Zubarev and Iskakova [62] (TZI model). In this approximation, the chain size is given by [4,24]

$$Q = \frac{2\phi z_0}{\sqrt{1+4\phi z_0}-1} \tag{16}$$

with

$$z_0 = \frac{e^{2\lambda}}{3\lambda^2}$$

and

$$\lambda = \frac{\pi^2}{36}\frac{M_s^2 D^6}{(D+D_{ss})^3 k_B T}.$$

As indicated earlier, this model is valid only for rigid chains. In the search for a more general description, Mendelev and Ivanov [60] introduced the so-called MI model, which is also valid for flexible chain aggregates. In the MI model, the chain size has the same dependence as in Eq. (16), except that now

$$z_0 = \frac{e^{2\lambda}}{3\lambda^3}\{1-\exp^{-\lambda}\}.$$

It is interesting to note that this expression is equivalent to that obtained by de Gennes and Pincus for the infinite dipolar interaction limit [63]. In the MI model, initial magnetic susceptibility is given by [60]

$$\chi = \chi_i \frac{1+p_0\kappa(\lambda/2)}{1-p_0\kappa(\lambda/2)}, \tag{17}$$

where

$$p_0 = \frac{1+2Z_0\phi-\sqrt{1+4Z_0\phi}}{2Z_0\phi}$$

and $\kappa(x)$ is a correlation coefficient that describes the zero field orientational correlations between the magnetic moments of interaction particles, which is given by a Langevin function,

$$\kappa\left(\frac{\lambda}{2}\right) = \coth\frac{\lambda}{2} - \frac{2}{\lambda}.$$

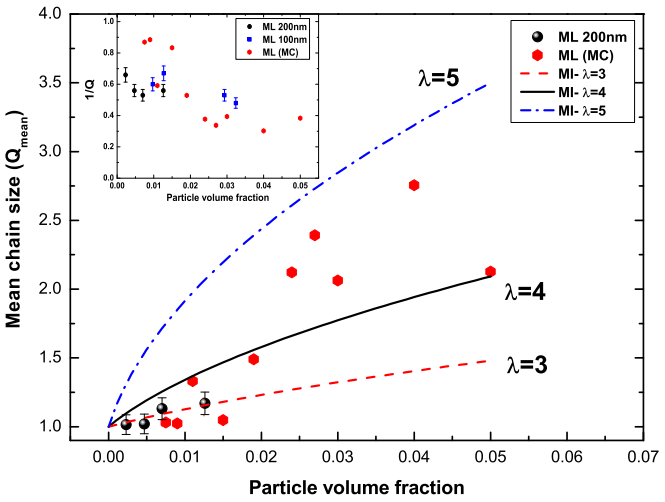

FIG. 7. Experimentally derived mean chain size Q_{mean} (circles) for the 200-nm sample and Monte Carlo simulation results (hexagons). The solid, dashed, dotted, and dashed-dotted lines represent theoretical values obtained following the Mendelev-Ivanov model [60]. In the inset, the inverse of the agglomerate mean value $(1/Q)$ as a function of the particle volume fraction. Experimental data are represented by black spheres (200-nm liposome sample) and blue squares (200-nm liposome sample) while Monte Carlo simulations are respresented by red hexagons.

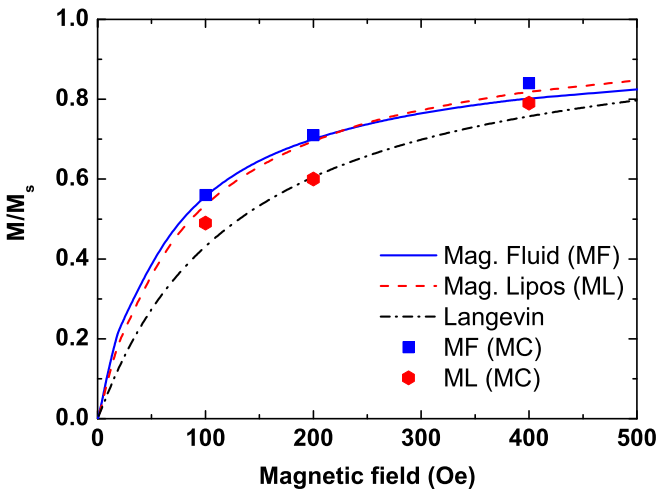

FIG. 8. Comparison between experimental data (dashed and solid lines), Langevin model (dashed-dotted line), and MC simulation (symbols) for the field dependence of the reduced magnetization $(\frac{M}{M_z})$ for a system considering a particle volume fraction of 0.01.

This expression for the susceptibility is equivalent to that obtained for the TZI model [61,62] when a very high dipolar interaction term is considered. This is a direct consequence of the fact that the Langevin function saturates, i.e., tends to the unity value, at this regime. Considering our magnetic nanoparticle mean diameter (14 nm) and $M_s = 226$ emu/cm^3 we obtain $\lambda_{\text{exp}} \approx 0.74$. In principle, this model is valid for λ greater than 1, which is larger than the calculated value. Alternatively, λ can be extract for a given sample using the log-normal distribution property. It is important to mention that that the dispersity of λ is 3 times higher than the one found for the particle diameter. From our size distribution we have found a mean value of $\lambda_{\text{mean}} = 1.14$, which would indicate that the particles do not interact strongly.

The mean chain size (Q_{mean}) concentration is defined as

$$Q_{\text{mean}} = Q f_{\text{agg}} + Q_{\text{mon}}(1 - f_{\text{agg}}),$$

where $Q_{\text{mon}} = 1$, since it is an isolated nanoparticle and f_{agg} is the fraction of aggregates. This later value is obtained from the comparison of the analysis of the SMB and magnetization data from which we extract the total number of nanoparticles. Q_{mean} as a function of the particle volume fraction for the 200-nm magnetoliposome (black spheres) and from the Monte Carlo simulations (red hexagons) is shown in Fig. 7. In agreement with our previous analysis, the mean chain size increases for higher volume fractions. Again, good agreement between experimental derived data and simulation results was achieved for lower particle concentrations. In addition, we have also compared our results with the Mendelev-Ivanov model (MI) [60] with distinct interaction parameter values (λ). The theoretical values are indicated by solid, dashed, dotted, and dashed-dotted lines. It is clear from this figure that nanoparticles trapped in a magnetoliposome are in a highly interacting situation. This can be numerically represented by the obtained λ values that better fit the experimental ($\lambda = 3$) data. It is important to mention that the Monte Carlo simulated values do not present a smooth behavior. This is probably related to the small number of nanoparticles entrapped in each liposome, especially at low concentration limits.

Having established that the flexible chain model can properly describe our system, we have used it in order to analyze our experimental data and Monte Carlo simulations. Figure 8 shows the field dependence of the reduced magnetization curves $(\frac{M}{M_s})$ of some of our samples, namely the magnetic fluid (solid line) and the magnetoliposome (dashed line) for a particle volume fraction close to 0.01. For comparison the calculated noninteracting Langevin curve (dashed-dotted line) for the sample parameters is also shown. The experimental data clearly indicate a highly interacting system since both ferrofluid and magnetoliposome appears to orient more rapidly than the Langevin case. At low field the response of the colloid is higher, while above a field of the order of 200–300 Oe the magnetoliposome starts to saturate faster. Our Monte Carlo simulation, indicated by symbols, correlate well specially at higher field limits.

In the determination of the susceptibility of magnetoliposomes at very low particle concentrations, the magnetic signal of the sample has diamagnetic (liquid carrier and liposome) and superparamagnetic contributions. The later is used to extract information of the susceptibility. In Fig. 9 the initial susceptibility as function of particle volume fraction for the magnetic fluid and magnetoliposome samples is shown. Open squares represent the magnetic fluid and spheres the magnetoliposome experimental data, while closed squares the magnetic fluid and closed hexagons the magnetoliposome Monte Carlo simulations. Experimentally, we found a lower susceptibility for the magnetoliposome samples in comparison with the magnetic fluid. The dashed-dotted line represents the Langevin model considering the sample parameters. The experimental data for both magnetic fluid and magnetoliposome differ considerably from the expected noninteracting

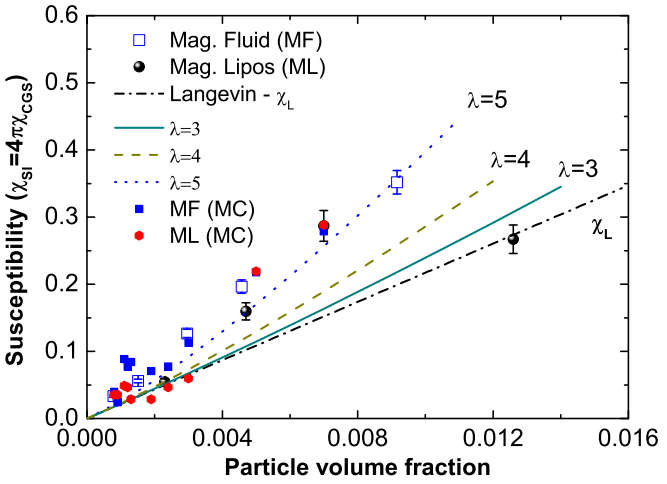

FIG. 9. Initial susceptibility as function of particle volume fraction for magnetic fluid (squares) and magnetoliposomes (spheres). The red line represents a Langevin calculation.

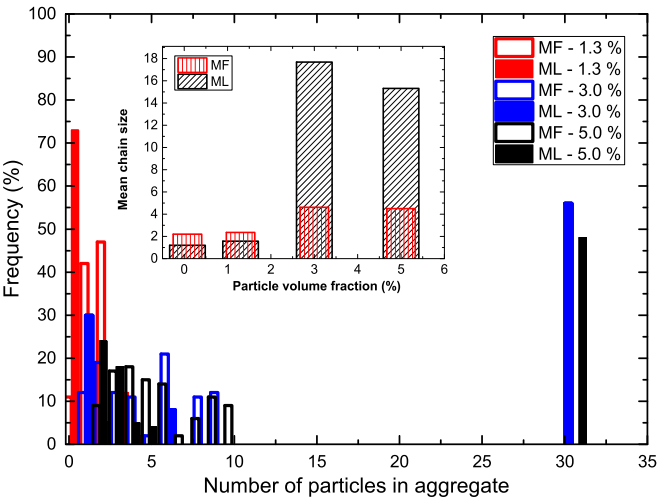

FIG. 10. Histograms of the cluster size distribution for the magnetic fluid (MF) and magnetoliposome samples (ML), for the 0.0013, 0.03, and 0.05 particle volume fractions (indicated in %), considering a 0.3-T magnetic field. In the inset, mean chain size as a function of particle volume fraction includes the 0.00075 (or 0.075%) data.

case (Langevin model) indicating, again, a highly interacting system. In order to compare available data with the flexible chain model, we simulated the susceptibility using Eq. (17) and different interaction parameters. The solid, dashed, and dotted lines are calculations using the MI model for distinct λ values, i.e., λ =3, 4, and 5, respectively. Good aggreement with the data is achieved for the highest λ value. Although the value found from this analysis is distinct from the chain size analysis reported before, it is possible to extract from both models that the samples have aggregates. In contrast with the experimental value, the MC simulations of the magnetic fluids approaches the Langevin model. The magnetoliposome MC simulations, on the other hand, is in good aggrement with the experiental data indicanting a high interacting system.

Our theoretical discussion was based on the MI model that is mainly valid for monodisperse colloids, while our samples are polydisperse in nature. Although there is a model, which was proposed by Ivanov and Kantorovich [64], where the chain formation process considers the *polydispersity* by assuming that a real sample can be approximated by a bidisperse system, we have not considered this approach. We understand that this later proposition is certainly a better approach when compared the the monodisperse one. However, it is quite complex. In principle, if one assumes a given particle configuration with large particles in the center of the aggregate and small ones at the edge, it is possible to extract information of these system. However, there is no guarantee that this configuration will be present in our samples. In our opinion, without cryogenic transmission electron microscopy pictures, such as those reported by Butter and coworkers [65], to give support for a typical aggregate configuration choice of a colloid sample, such an approach could be seen experimentally aa a bit speculative. Therefore, we prefer to use the polydispersity analysis as reported in our work, which is based on an average chain size (see Sec. II).

Next we compare the chain distributions in two situations: nonconfined magnetic fluid, which is usually the subject of most of the works in the literature, and the magnetoliposome case, i.e., when nanoparticles are entrapped in the liposome. Histograms of the cluster size distribution for the magnetic fluid (MF) and magnetoliposome samples (ML), for the 0.0013, 0.03, and 0.05 particle volume fractions (indicated in %), considering a 0.3-T magnetic field are shown in Fig. 10. The histograms are based on the final particle configurations. In the inset, the main chain size as a function of the particle volume fraction for MF and ML is also presented, including a lower-volume-fraction result.

Our simulation data indicate that, at lower volume fractions, ML presents a lower aggregate formation. This is consistent with our susceptibility results, since at lower magnetic fields the susceptibility of the ML approaches the Langevin function, which represents a noninteracting system. Our simulation results are also consistent with with the experimental indication, at lower volume fractions, of a lower susceptibility for ML when compared to MF.

Our results indicate that, for higher concentrations, ML presents a higher degree of aggregation. Indeed, more complex chain distributions, including clusters of the order of 30 particles, are observed for the ML samples with particle volume fractions of 0.03 and 0.05. This is consistent with the ferrofluid simulations under plate confinement reported by Richardi and Weis [66]. For the nonconfined MF, on the other hand, our calculations show distributions that are similar to those obtained by Osipov and coworkers [67]. Our simulation data indicate that, for ML, there is a particle volume fraction-dependent transition from a situation of few aggregates to more complex system. Indeed, a complete study about the influence of such complex structures might be an interesting topic. An example of possible changes in the properties of MF due to the formation of complex structures was recently given by Kantorovich *et al.* [68], who found a decrease in the initial susceptibility in dipolar fluids when temperature decreases due to the formation of ringlike structures (flux closure particle arrangements). In ML this behavior might be relevant at very high particle concentration, when the nanoparticles are

entrapped into the vesicles. One might expect change in their magnetic properties, which could have implications in the biomedical field. However, this is not the focus of this work and will be left for future investigations.

V. CONCLUSIONS

In this work we have developed and implemented a new approach for the study of magnetoliposomes using the Monte Carlo method. Our model is based on interaction among nanoparticles considering various particle-particle interaction terms, while the interaction between nanoparticles and the lipid bilayer is represented by a ionic repulsion electrical surface potential that depends on the nanoparticle-lipid bilayer distance and the concentration of ions in the solution. In our experimental approach, magnetoliposomes containing a different amount of magnetic particles encapsulated were prepared by thin lipid film hydration followed by extrusion. The nanosystems were investigated by transmission electron microscopy, vibrating sample magnetometer, dynamic light scattering, nanoparticle tracking analysis, and SMB. SMB allowed us to extract information about the nanoparticle self-organization inside the vesicles. In addition, magnetization and susceptibility data are also accessed. A direct comparison between experimental and simulation data allows us to validate our MC implementation. Our simulations suggest that at lower volume fractions, ML presents a lower aggregate formation, while for higher concentrations, ML presents a higher degree of aggregation when compared to MF.

ACKNOWLEDGMENTS

The authors acknowledge financial support from the Brazilian agencies FAPESP (Project No. 2012/50680-5), FAPEG, CNPq, and CAPES. We also acknowledge LabMic for the use of TEM facilities.

[1] K. Raj and R. Moskowitz, J. Magn. Magn. Mater. **85**, 233 (1990).
[2] V. Segal, A. Rabinovich, D. Nattrass, K. Raj, and A. Nunes, J. Magn. Magn. Mater. **215-216**, 513 (2000).
[3] H. L. G. Couto, N. B. Marcelino, and F. R. Cunha, Magnetohydrodynamics **43**, 421 (2007).
[4] M. T. A. Eloi, J. L. Santos, P. C. Morais, and A. F. Bakuzis, Phys. Rev. E **82**, 021407 (2010).
[5] R. V. Mehta, R. Patel, R. Desai, R. V. Upadhyay, and K. Parekh, Phys. Rev. Lett. **96**, 127402 (2006).
[6] J. Philip, J. M. Laskar, and B. Raj, Appl. Phys. Lett. **92**, 221911 (2008).
[7] C. T. Yavuz, J. T. Mayo, W. W. Yu, A. Prakash, J. C. Falkner, S. Yean, L. Cong, H. J. Shipley, A. Kan, M. Tomson, D. Natelson, and V. L. Colvin, Science (NY) **314**, 964 (2006).
[8] J. W. Bulte, T. Douglas, B. Witwer, S. C. Zhang, E. Strable, B. K. Lewis, H. Zywicke, B. Miller, P. van Gelderen, B. M. Moskowitz, I. D. Duncan, and J. A. Frank, Nat. Biotechnol. **19**, 1141 (2001).
[9] D. E. Sosnovik, M. Nahrendorf, and R. Weissleder, Circulation **115**, 2076 (2007).
[10] J. R. McCarthy and R. Weissleder, Adv. Drug Deliv. Rev. **60**, 1241 (2008).
[11] M. G. Harisinghani, J. Barentsz, P. F. Hahn, W. M. Deserno, S. Tabatabaei, C. H. van de Kaa, J. de la Rosette, and R. Weissleder, N. Engl. J. Med. **348**, 2491 (2003).
[12] R. K. Gilchrist, R. Medal, W. D. Shorey, R. C. Hanselman, J. C. Parrott, and C. B. Taylor, Ann. Surg. **146**, 596 (1957).
[13] A. Jordan, R. Scholz, P. Wust, H. Fähling, J. Krause, W. Wlodarczyk, B. Sander, T. Vogl, and R. Felix, Int. J. Hypertherm. **13**, 587 (1997).
[14] S. J. DeNardo, G. L. DeNardo, A. Natarajan, L. a. Miers, A. R. Foreman, C. Gruettner, G. N. Adamson, and R. Ivkov, Soc. Nucl. Med. **48**, 437 (2007).
[15] L. C. Branquinho, M. S. Carrião, A. S. Costa, N. Zufelato, M. H. Sousa, R. Miotto, R. Ivkov, and A. F. Bakuzis, Sci. Rep. **3**, 2887 (2013).
[16] H. F. Rodrigues, F. M. Mello, L. C. Branquinho, N. Zufelato, E. P. Silveira-Lacerda, and A. F. Bakuzis, Int. J. Hypertherm. **29**, 752 (2013).
[17] K. M. Krishnan, IEEE Trans. Magn. **46**, 2523 (2010).
[18] M. Cuyper and M. Joniau, Eur. Biophys. J. **15** 311 (1988).
[19] M. Babincová, P. Cicmanec, V. Altanerová, C. Altaner, and P. Babinec, Bioelectrochemistry (Amsterdam) **55**, 17 (2002).
[20] H. Nobuto, T. Sugita, T. Kubo, S. Shimose, Y. Yasunaga, T. Murakami, and M. Ochi, Int. J. Cancer **109**, 627 (2004).
[21] T. Ruysschaert, L. Paquereau, M. Winterhalter, and D. Fournier, Nano Lett. **6**, 2755 (2006).
[22] L. Zhang and S. Granick, Nano Lett. **6**, 694 (2006).
[23] E. R. Cintra, F. S. Ferreira, J. L. Santos Junior, J. C. Campello, L. M. Socolovsky, E. M. Lima, and A. F. Bakuzis, Nanotechnology **20**, 045103 (2009).
[24] A. F. Bakuzis, L. C. Branquinho, L. Luiz e Castro, M. T. de Amaral e Eloi, and R. Miotto, Adv. Colloid Interface Sci. **191-192**, 1 (2013).
[25] V. Filipe, A. Hawe, and W. Jiskoot, Pharm. Res. **27**, 796 (2010).
[26] A. O. Ivanov, S. S. Kantorovich, E. N. Reznikov, C. Holm, A. F. Pshenichnikov, A. V. Lebedev, A. Chremos, and P. J. Camp, Phys. Rev. E **75**, 061405 (2007).
[27] M. Rasa, Eur. Phys. J. E **2**, 265 (2000).
[28] T. Du and W. Luo, Appl. Phys. Lett. **72**, 272 (1998).
[29] A. F. Bakuzis, K. Skeff Neto, P. P. Gravina, L. C. Figueiredo, P. C. Morais, L. P. Silva, R. B. Azevedo, and O. Silva, Appl. Phys. Lett. **84**, 2355 (2004).
[30] M. Xu and P. J. Ridler, J. Appl. Phys. **82**, 326 (1997).
[31] K. Binder, ed., *The Monte Carlo Method in Condensed Matter Physics*, Topics in Applied Physics, Vol. 71 (Springer-Verlag, Heidelberg, 1992), p. 392.
[32] N. Metropolis, A. W. Rosenbluth, M. N. Rosenbluth, A. H. Teller, and E. Teller, J. Chem. Phys. **21**, 1087 (1953).
[33] M. P. Allen and D. J. Tildesley, *Computer Simulation of Liquids* (Oxford University Press, Oxford, 1989), p. 408.
[34] W. K. Hastings, Biometrika **57**, 97 (1970).

[35] L. L. Castro, G. R. R. Gonçalves, K. S. Neto, P. C. Morais, A. F. Bakuzis, and R. Miotto, Phys. Rev. E **78**, 061507 (2008).
[36] L. Castro, M. Dasilva, A. Bakuzis, and R. Miotto, J. Magn. Magn. Mater. **293**, 553 (2005).
[37] H. Hamaker, Physica **4**, 1058 (1937).
[38] J. N. Israelachvili, *Intermolecular and Surface Forces*, 3rd ed. (Academic Press, New York, 2011), p. 704.
[39] E. M. Lifshitz, J. Exp. Theor. Phys. **2**, 73 (1956).
[40] I. Dzyaloshinskii, E. Lifshitz, and L. Pitaevskii, Adv. Phys. **10**, 165 (1961).
[41] D. P. Lide, ed., *CRC Handbook of Chemistry and Physics*, 88th ed. (CRC Press, Boca Raton, FL, 2007), p. 2640.
[42] D. G. Archer and P. Wang, J. Phys. Chem. Ref. Data **19**, 371 (1990).
[43] P. Schiebener, J. Straub, J. M. H. Levelt Sengers, and J. S. Gallagher, J. Phys. Chem. Ref. Data **19**, 677 (1990).
[44] T. Tepper, C. Ross, and G. Dionne, IEEE Trans. Magn. **40**, 1685 (2004).
[45] E. Mackor, J. Colloid Sci. **6**, 492 (1951).
[46] L. L. Castro, R. Miotto, and A. F. Bakuzis, J. Appl. Phys. **99**, 08S101 (2006).
[47] R. F. Ziolo, Eur. Cells Mater, **3**, 92 (2002).
[48] M. A. J. Hodenius, T. Niendorf, G. A. Krombach, W. Richtering, T. Eckert, H. Lueken, M. Speldrich, R. W. Günther, M. Baumann, S. J. H. Soenen, M. De Cuyper, and T. Schmitz-Rode, J. Nanosci. Nanotechnol. **8**, 2399 (2008).
[49] E. Tombácz, D. Bica, A. Hajdú, E. Illés, A. Majzik, and L. Vékás, J. Phys.: Condens. Matter **20**, 204103 (2008).
[50] S. Kumar, C. Ravikumar, and R. Bandyopadhyaya, Langmuir **26**, 18320 (2010).
[51] D. Voet and J. G. Voet, *Biochemistry*, 4th ed. (John Wiley & Sons, New York, 2010), p. 1520.
[52] M. Kanduč, E. Schneck, and R. R. Netz, Langmuir **29**, 9126 (2013).
[53] S. A. Tatulian, J. Phys. Chem. **98**, 4963 (1994).
[54] J. N. Israelachvili and H. Wennerstroem, J. Phys. Chem. **96**, 520 (1992).
[55] V. M. Aguilella, S. Mafé, and J. A. Manzanares, Chem. Phys. Lipids **105**, 225 (2000).
[56] D. Taylor, O. Oliveira, and H. Morgan, Chem. Phys. Lett. **161**, 147 (1989).
[57] S. O. Nielsen, C. F. Lopez, G. Srinivas, and M. L. Klein, J. Phys.: Condens. Matter **16**, R481 (2004).
[58] M. A. Katsoulakis, P. Plecháč, and A. Sopasakis, SIAM J. Numer. Anal. **44**, 2270 (2006).
[59] E. Amstad, J. Kohlbrecher, E. Müller, T. Schweizer, M. Textor, and E. Reimhult, Nano Lett. **11**, 1664 (2011).
[60] V. S. Mendelev and A. O. Ivanov, Phys. Rev. E **70**, 051502 (2004).
[61] A. O. Tsebers, Magnetohydrodynamics **10**, 135 (1974).
[62] A. Yu Zubarev and L. Yu. Iskakova, Phys. Rev. E **65**, 061406 (2002).
[63] P. G. de Gennes, P. A. Pincus, and P. G. de Gennes, Phys. Kondens. Mater. **11**, 189 (1970).
[64] A. O. Ivanov and S. S. Kantorovich, Phys. Rev. E **70**, 021401 (2004).
[65] K. Butter, P. H. H. Bomans, P. M. Frederik, G. J. Vroege, and A. P. Philipse, Nat. Mater. **2**, 88 (2003).
[66] J. Richardi and J.-J. Weis, J. Chem. Phys. **135**, 124502 (2011).
[67] M. A. Osipov, P. I. C. Teixeira, and M. M. Telo da Gama, Phys. Rev. E **54**, 2597 (1996).
[68] S. Kantorovich, A. O. Ivanov, L. Rovigatti, J. M. Tavares, and F. Sciortino, Phys. Rev. Lett. **110**, 148306 (2013).